Haggren, Tuomas; Anttu, Nicklas; Mäntynen, Henrik; Tossi, Camilla; Kim, Maria; Khayrudinov, Vladislav; Lipsanen, Harri

Management of light and scattering in InP NWs by dielectric polymer shell

Published in:
Nanotechnology

DOI:
10.1088/1361-6528/ab9aec

Published: 18/09/2020

Document Version
Peer-reviewed accepted author manuscript, also known as Final accepted manuscript or Post-print

Nanotechnology

ACCEPTED MANUSCRIPT

Management of light and scattering in InP NWs by dielectric polymer shell

To cite this article before publication: Tuomas Haggren *et al* 2020 *Nanotechnology* in press https://doi.org/10.1088/1361-6528/ab9aec

IOP Publishing Journal Title
Journal **XX** (XXXX) XXXXXX https://doi.org/XXXX/XXXX

Management of light and scattering in InP NWs by dielectric polymer shell

Tuomas Haggren†*, Nicklas Anttu, Henrik Mäntynen, Camilla Tossi, Maria Kim°, Vladislav Khayrudinov and Harri Lipsanen.

Department of Electronics and Nanoengineering, Micronova, Aalto University, P.O. Box 13500, FI-00076, Finland
† Present address: Department of Electronic Materials Engineering, Research School of Physics and Engineering, The Australian National University, Canberra, ACT 2601, Australia.
° Present address: Ioffe Institute, Polytechnicheskaya 26, 194021 St.Petersburg, Russia

* Corresponding author E-mail: tuomas.haggren@anu.edu.au

Received xxxxxx
Accepted for publication xxxxxx
Published xxxxxx

Abstract

Understanding and management of light is of great importance for nanoscale devices. This report demonstrates enhanced absorption, photoluminescence and scattering in InP nanowires when coated with dielectric polymer shell. The shells increase absorption and emission by a factor of ~2 and photoluminescence by a factor of ~4. A thorough optical characterization is provided, including reflectance, transmission, luminescence and scattering to incident and transmitted directions. From this characterization, we derive the distribution of absorbed light within the structure (InP nanowires, Au seed particles and the substrate). Additionally, reflectance, transmission and emission are shown to become increasingly diffuse with the dielectric shells. The results are thought to provide better understanding in light-matter interaction in nanostructures, as well as to provide valuable tools for light and scattering management in nanoscale optoelectronics.

Keywords: diffuse, specular, nanowire, NW, emission, scattering, transmittance, absorptance, light trapping, light distribution, dielectric shell, photoluminescence

1. Introduction

Semiconductor nanowires are a promising pathway to realize various next-generation optoelectronic devices. One of their key benefits is their antenna-like shape that greatly impacts their interaction with light [1,2]. On the other hand, the nanowire morphology and dimensions govern this interaction, and can result for example in weak or strong absorption with the same material system [3,4]. Therefore, understanding the behavior of light in nanowire arrays is of great importance, and perhaps even more so is the possibility to tune the behavior.

Semiconductor nanowires are typically grown on semiconducting substrates, such as Si and InP, which are suitable platforms for device fabrication and hence interesting. However, such substrates are opaque and limit the possibilities of optical characterization. Reduced reflectance is often reported for semiconductor NW arrays [5–7], which however does not necessarily imply high absorption. Instead, the NW arrays may simply promote light propagation into the substrate, where it may not be helpful for devices where the active region comprises NWs [7–9]. In terms of optical characterization, a more complete picture is acquired by using a transparent substrate that enables NW growth on materials such as glass [10], GaN [11,12] or transparent conductive oxides [13,14]. Other approaches include peeled-off NWs embedded in polymer film[4,15], which however requires relatively difficult processing steps.

Besides understanding light-NW interaction, its management or tuning the behavior is of great importance for

NW optoelectronics. Both light absorption [3,4,8,9] and light scattering [16] have been previously managed by tuning the NW dimensions, relative positions and/or orientations. This approach however typically requires position-controlled NW fabrication and delicate tuning of the array parameters [3]. Another approach for light management is the use of dielectric shell on the NWs that has been shown to significantly improve absorption [17,18], enhance device efficiency [19] and increase scattering cross-section [20]. Furthermore, the use of an dielectric shell may provide higher absorption with lower fill factor compared to arrays composed of NWs only [21].

In this work, we study InP nanowires grown directly on glass, which allows studying both reflectance and transmittance, as well as scattering to reflected and transmitted directions. The present work is also the first to study scattering in detail on transparent substrates. Light and scattering management in the InP NW ensembles is performed by conformal parylene-C polymer coating. It is a low-cost material with facile and gentle room-temperature deposition, and is used in numerous applications such as NW optoelectronics [22], various flexible devices (*e.g.* NWs [23,24], nanotubes [25], 2D materials [26], organic transistors [27]), as corrosion and moisture barrier [23,24], and as conformal planarization material [22]. As such, parylene-C is more versatile compared to materials deposited *e.g.* by atomic layer deposition (ALD) or sputtering. Here, parylene-C as a coating is shown to enhance absorption, photoluminescence (PL) properties, scattering and diffuse reflection, transmission and emission. Enhanced absorption and PL suggest that the parylene-C shell is beneficial for NW optoelectronics [8,9], while the enhanced scattering may be utilized *e.g.* in random lasers [28] and superlenses [29]. The results shown here provide important understanding in how the incident light is distributed between different parts of the NWs and the substrate, and provide further insights on dielectric shell effects on scattering and diffuse/specular reflectance, transmission and emission. As such, the study delivers valuable tools for nanoscale engineering using dielectric shells.

2. Methods

The NWs were grown in a horizontal-flow metalorganic vapor phase epitaxy (MOVPE) reactor using colloidal Au nanoparticles (BBI International) as seeds for vapor-liquid-solid growth. The Au seed particles were nominally 40nm in diameter, yielding ≈40nm thick NWs. The growth was initiated by simultaneously switching on trimethylindium (TMIn) and tertiarybutylphosphine (TBP) sources at 440 °C, with the flows of 5.6 µmol/min and 1100 µmol/min, respectively. The growth time was 200 s, which resulted in the NW length of ≈5 µm. As the growth substrate, a single glass slide was used, which was cleaved into four 8 mm × 8mm squares. Therefore, the growth conditions were identical for the different samples, while Au seed particle density and thus NW density varied slightly between the samples.

The optical characterization included reflectance (R), transmittance (T) and absorptance (A) measurements using two different setups. R and T was measured from all samples prior to and after the parylene-C depositions. In one setup, R, T and A were measured using an integrating sphere, and the NWs were illuminated at 8° (see supporting info Fig. S1 for illustration). For A, the sample was glued to a thin metal rod and then placed inside the sphere. Wavelength range of 400 – 900 nm was measured with Si detector, and wavelength range of 930 – 1600 nm was measured with InGaAs detector. Another setup was used for R and T scattering studies. In that setup, the samples were illuminated through an objective lens, and the light was collected either through the same lens for reflectance, or by a lens or an integrating sphere for transmittance measurement (see Fig.S2).

Parylene-C spray coating (SCS Labcoter 2 Parylene Deposition System) was used to deposit the conformal polymer layer to form shells on the InP NWs. The deposition took place at room temperature under vacuum conditions. Parylene thickness was verified using ellipsometry. For the R, T, A and photoluminescence measurements, four samples were coated individually with nominally 58 nm, 106 nm, 215 nm and 354 nm of parylene-C, measured, and subsequently additional 390 nm was deposited on each sample. The resulting shell thickness range was therefore 58 nm – 744 nm. Similarly fabricated four samples were used for scattering studies with nominal thicknesses of 0 nm, 50 nm, 100 nm and 200nm.

Macro-PL, with a spot size of approximately 100 µm in diameter, was measured using continuous-wave laser with 532 nm wavelength and 12.6 mW power for excitation, and the spectra were collected using a monochromator, lock-in amplifier and Si photodetector. To study the effect of parylene-C coating on PL, the same sample was measured before and after the deposition. In micro-PL measurements, 532 nm laser was used for excitation and the acquisitions were made with a Witec alpha300 microscope. Nanowire morphology and the coating conformality were studied by scanning electron microscopy (SEM) (Zeiss Supra 40).

3. Results and discussion

3.1 Morphology and structure

Fig. 1 shows SEM images of the NWs before and after the parylene-C coating. The NWs are straight and grow in random directions. Based on our earlier studies on InP NWs on glass, the crystal structure is predominantly zinc-blende with frequent twin planes [10]. The parylene-C deposition takes place conformally on all surfaces, and results in an even diameter over the whole NW length and over any surface features [22]. The refractive index of parylene- C ($n \cong 1.65$) [30,31] is between that of InP (≈3.5 – 4.2 in the visible range) and air ($n \cong 1$), and is therefore expected to reduce dielectric screening between the surrounding air and the NW and enhance light absorption to the small-diameter NWs [17]. The structure schematic in Fig. 1c shows also various processes that incoming photons may undergo; each of these processes is examined in this work.

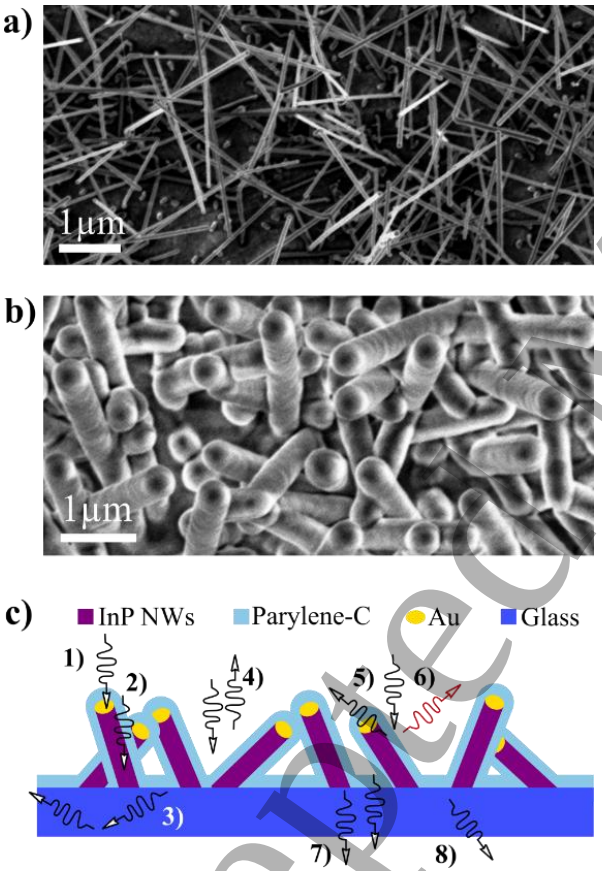

Figure 1: SEM images from uncoated InP NWs (a) and from NWs with 200 nm parylene-C coating (b), and a schematic of the structure (c) with various alternatives shown for incoming photons in the structure: absorption in Au (1), absorption in InP (2), trapping in glass slide (3), specular reflection (4), diffuse reflection (5), diffuse emission (after absorption in InP) (6), specular transmission (7) and diffuse transmission (8).

3.2 Reflectance, transmittance and absorptance

Fig. 2 shows values measured with integrating sphere for reflectance (R), transmittance (T) and 1-R-T from the 4 samples described in the experimental section. The values shown in Fig. 2 represent averages over wavelength range 400 – 900 nm, which is absorbed by InP and as such of interest in NW optoelectronics (Fig. S3 shows wavelength range 930 - 1600 nm). The reflectance measurements are discussed here first. Absolute reflectance values are shown in Fig. 2a and relative changes in Fig. 2d. The parylene-C coating had a minor effect on the absolute reflectance shown in Fig. 2a, while the relative change reached ≈1.5 at a shell thickness of ≈215 nm. The increase in reflectance is in contrast to previous reports on ordered NW arrays with dielectric shells [17,21] and seems counterintuitive. However, since the absolute changes are small, the increased reflectance can be attributed to increased scattering of light to angles that promote internal reflection at the glass back-surface, that is, beyond the critical angle (scattering is discussed later in this paper). The light trapped thus is more likely to escape from the front surface, where the rough NW/parylene-C matrix could enable out-coupling of light that propagates even beyond the critical angle of a planar glass-air interface. Thus, stronger scattering results in a slight increase in observed reflectance. The saturation of the reflectance at higher parylene-C shell thicknesses is attributed to the parylene-C filling the space between the NWs, resulting in a more homogenous layer and reduced scattering.

In contrast to reflectance, the transmittance is strongly affected by the parylene-C shells. As a result, the 1-R-T is largely governed by transmittance, and therefore, 1-R-T and T are discussed here together. The parylene-C coating decreases T and increases 1-R-T, initially rapidly up to shell thickness of 215 nm, where the 1-R-T is increased by ≈50 % (relative increase). This trend corresponds to reduced dielectric screening in previous reports [17], and shows that the polymer shells can be used in a similar fashion as oxide shells deposited by sputtering [18] or ALD [17]. After the thickness of ≈200 nm, the transmittance and the 1-R-T remain roughly constant. However, closer scrutiny on individual samples (shown with different symbols in Fig. 2) suggests that 1-R-T peaks between 100 - 300nm and decreases slightly with the thickest shells. Previously, similar trend has been attributed to a cross-sectional resonance condition, which peaks at certain thicknesses and is reduced when thickness is increased further, especially when the shell material fills the space between the NWs completely [17].

In the following, the light distribution and propagation in the structure is discussed, with the focus on wavelength range absorbed by InP. In that range, the 1-R-T values correspond to light that is 'lost' in three different categories: (i) absorption in InP, (ii) absorption in the Au seed particles and (iii) light

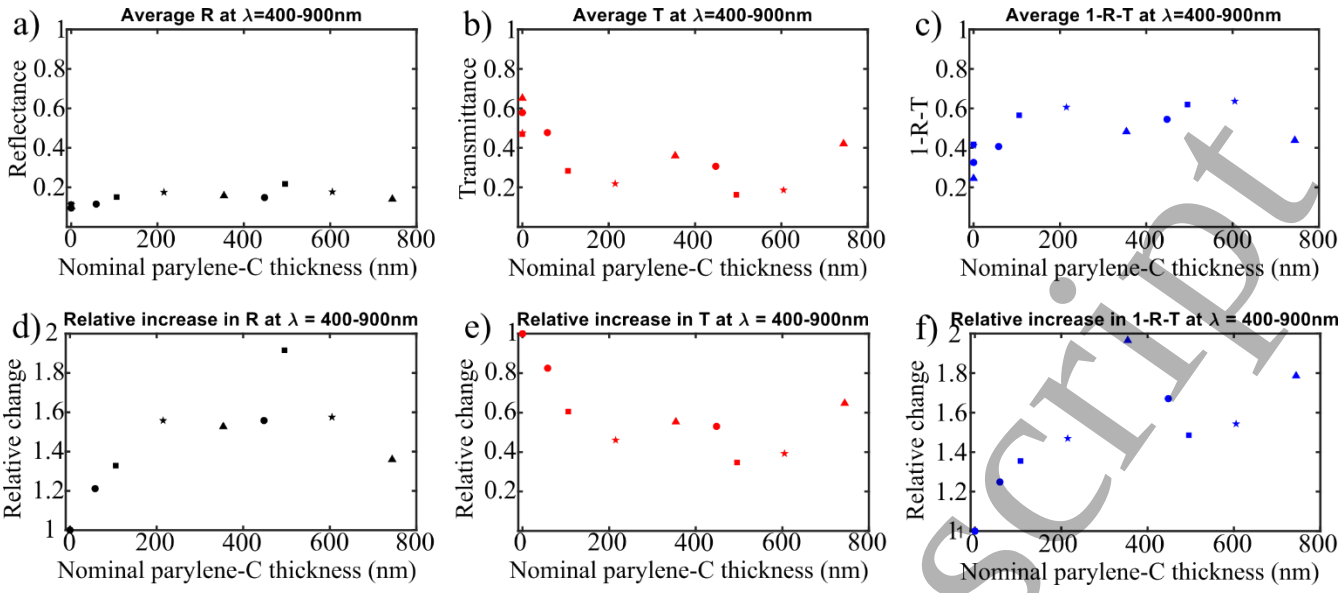

Figure 2: Absolute values for reflectance (a), transmittance (b) and 1-R-T (c), and relative change in R (d), T (e) and 1-R-T (f) from parylene-C coated InP NWs with different thicknesses. The values are averaged over the wavelength range 400 nm – 900 nm. The symbols represent four different samples on which parylene-C shells of varying thickness were deposited.

that becomes trapped in the glass substrate and subsequently escapes from its edges from where it does not enter our R and T measurements. The light-trapping in glass can occur when the photons are scattered to angles beyond the critical angle of total-internal-reflection condition. Any light that is trapped initially and subsequently escapes from the incident or transmitted sides is seen as reflection or transmission, respectively, and therefore is accounted for in the 1-R-T values. Fig. 3 shows approximated values and relative changes for these three categories with different parylene-C thicknesses, and the approximation methods are discussed below.

The absorption in InP is considered here first. Since InP is absorbing below ≈900 nm at room temperature and non-absorbing at longer wavelengths, comparing these two regions allows the estimation of absorption in InP from the 1-R-T measurements. Here, the InP absorption is estimated by assuming that at long wavelengths, the measured values correspond to absorption in Au and to light-trapping in glass. Thus, the InP absorption is obtained by deducting the mean value of 1-R-T $|_{\lambda > 930\text{nm}}$ from 1-R-T $|_{\lambda < 900\text{ nm}}$ (for clarity, sample-specific spectra are shown in Figs. S4-S5). This approximation assumes wavelength-independent Au-induced absorption and scattering (*i.e.* light-trapping in glass), which however is likely to result in underestimation on InP absorption. In the wavelength regime $\lambda < 900$ nm absorption in Au is expected to decrease due to considerable absorption in InP, and indeed relatively weak Au absorption at photon energies above the band gap has been reported for InGaP NWs [15]. On the other hand, scattering (which increases light trapping to glass) was found stronger at shorter wavelengths, as will be discussed later in this paper. Overall, while not perfectly accurate, the approximation is thought to provide reasonable values and to allow closer inspection of the light distribution in the structure.

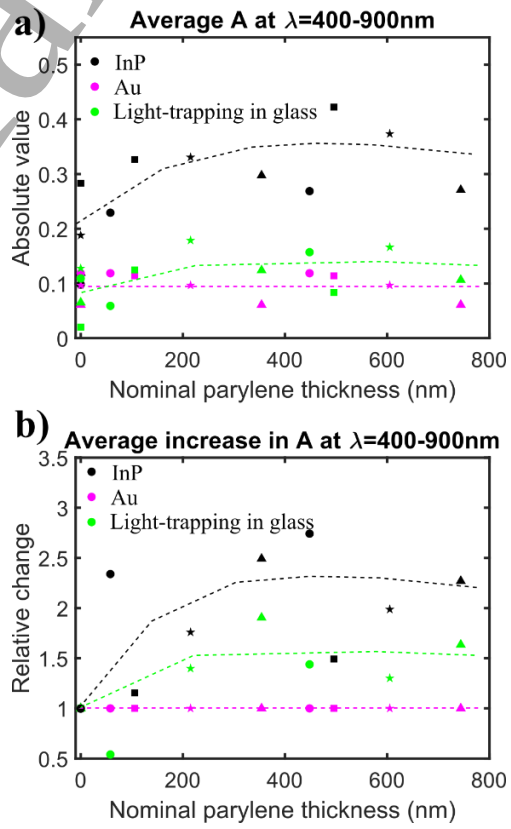

Figure 3: Absolute (a) and relative (b) increase in absorption in InP NW and in Au nanoparticle, and in light trapping to glass slide with different parylene-C thicknesses. The dashed lines serve as guides to the eye.

The absorption in Au seed particles at wavelengths $\lambda > 930$ nm was acquired either by measuring absorptance directly (where also the light trapped in glass slide is collected) or from 1-R-T measurements from uncoated NWs. These values were found to correspond closely to each other (see Fig. S6). This similarity suggests minimal light-trapping in glass slide without parylene-C shell. As mentioned above, the absorption in Au is assumed wavelength-independent and average absorption at $\lambda > 930$ nm is used in Fig. 3. As such, the values shown are likely underestimated due to reasons discussed above. Au nanoparticle removal was not attempted here due to possible detrimental effects on the ≈40nm thick NWs, such as surface etching and surface tension effects when the etching solution is removed. Finally, the light-trapping in glass is estimated by deducting absorption in InP and absorption in Au from the measured total 1-R-T values: light-trapping = (1-R-T) – A(Au) – A(InP).

Coming back to Fig. 3, several conclusions can be drawn from the dataset. First, majority of the photons entering the structure are absorbed by InP, while both Au absorption and light-trapping in glass have significant contributions. This suggest that absorption even in 40 nm Au particles is not negligible and may have detrimental impact on NW devices such as solar cells and LEDs. Second, for maximal benefit in InP absorption, already relatively thin parylene-C shell is sufficient. We would like to note here that the refractive index of parylene-C (≈1.65) is larger than *e.g.* ALD-based SiO_2 [32] and similar to ALD-based Al_2O_3 [33]. Therefore, the required parylene-C thickness for absorption enhancement is similar to, or even lower than, ALD-deposited conformal shells. Third, the relative increase in InP absorption is larger compared to the other components (a factor of ≈2 in InP absorption compared to a factor of ≈1.5 in total 1-R-T), *i.e.* for absorption in InP, the benefits of the shell are larger than what is apparent directly from the 1-R-T values.

3.3 Scattering

Next, the effects on scattering by the dielectric shell are discussed. While an integrating sphere collects in principle all of the reflected and transmitted light, light collection at different acceptance angles gives further insights on the interaction between light and the NW forest (see measurement schematic in Fig. S2). Figures 4a-b show transmittance spectra collected by either an optical lens or with an integrating sphere from 4 samples with nominally 0 – 200 nm parylene-C shells. This thickness region is of interest due to saturation of T and R after ≈200 nm thickness. The intensities in Fig. 4a-b are normalized to collected light without any sample in the beam path. The optical lens had approximately ≈15° collection angle and the integrating sphere ≈160° when the sample was sitting on the sphere entrance. Therefore, the 15° collection angle corresponds to light that undergoes little or no scattering while passing through the sample, and the 160° collection angle to practically all light that escapes from the glass slide (critical angle between glass and air being ≈42°).

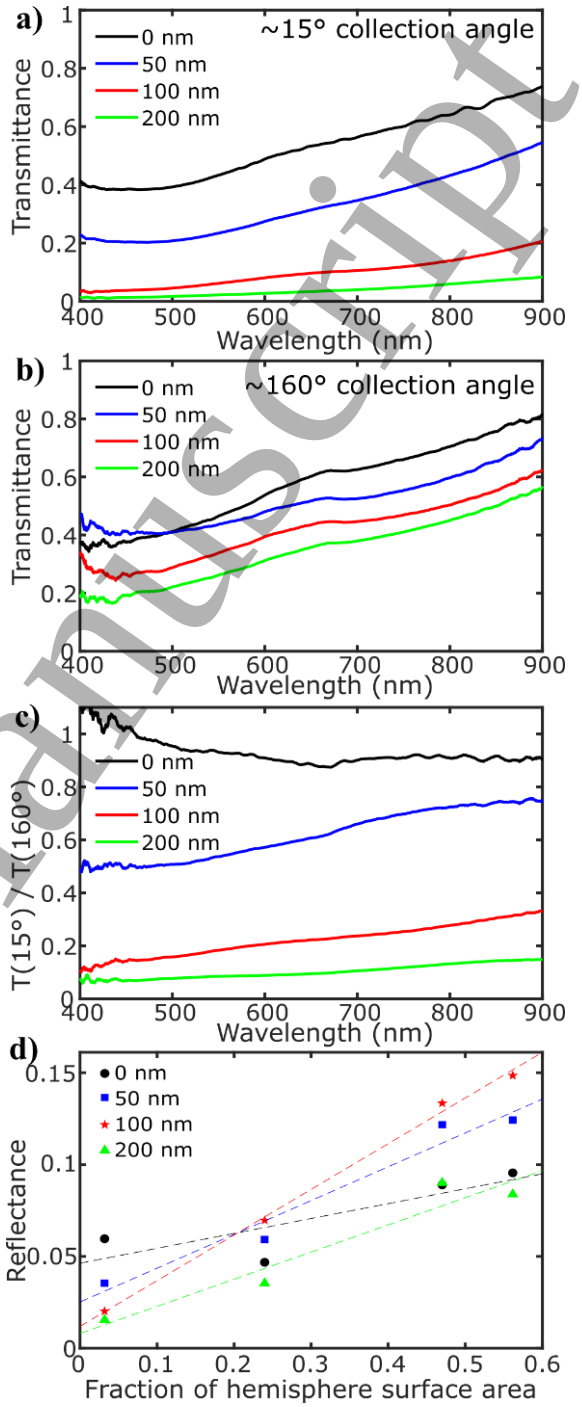

Figure 4: Transmittance from InP NWs with parylene-C shells collected with acceptance angles ≈15° (a) and ≈160° (b), and individual transmittance at ≈15° divided by corresponding transmittance at ≈160° (c); and reflectance measured at different acceptance angles corresponding to different fractions of hemisphere surface area, i.e., fractions of Lambertian diffuse reflection (d). The dashed lines in (d) serve as guides to the eye.

In Fig. 4a (light collection cone 15°), the collected light intensity decreases drastically when dielectric shell is applied on the NWs. On the other hand, the effect of the shell is clearly smaller when the light is collected with 160° acceptance angle (Fig. 4b). In other words, the proportion of light that escapes the glass slide at >15° is clearly higher when the dielectric shell is applied on the NWs, *i.e.*, the shell results in significantly increased scattering.

This effect is emphasized in more detail in Fig. 4c, where the following ratio is shown: light collected at 15°/ light collected at 160°. This is approximately the same as the fraction of specular transmittance / diffuse transmittance. Without the shell, the transmitted light is roughly 90 % specular. When the dielectric shell is applied, the fraction of specular transmittance decreases down to ≈10% with shell thickness of ≈200 nm. Clearly, the dielectric shell induces strong scattering, which is seen as significantly increased diffuse transmittance. Significant wavelength dependence is also observed in Fig. 4c, where shorter wavelengths have a smaller specular component, *i.e.*, the shorter wavelengths undergo stronger scattering. Such wavelength dependence is expected from Rayleigh scattering, and similar behavior has been reported previously for different NW diameters, where the thicker NWs induced stronger scattering, and the effect was more pronounced at short wavelengths. [16]

Reflectance for scattering studies was measured from 5 spots from each sample with 4 different objectives having numerical apertures of 0.25, 0.65, 0.85 and 0.9 (corresponding acceptance angles ≈29°, ≈81°, ≈116° and ≈128°, respectively). The illumination did not populate the entrance aperture of the objective completely, and therefore, the illumination was from a smaller angle than the collection. While this may affect the measurements to some degree, it was not analyzed in detail here. The acceptance angles correspond to fractions of spherical cap surface areas of 0.03, 0.24, 0.47 and 0.56, respectively, according to $A = 2\pi r^2(1-\cos(\theta))$, where θ is half of the acceptance angle values. Assuming Lambertian reflectance, the photons are divided equally to the hemisphere surface area. Therefore, these fractions correspond to fractions of Lambertian reflectance. Fig. 4d shows R collected from coated and uncoated NWs with different acceptance angles (averaged over 400 nm – 900 nm, normalized to reflectance from an Ag mirror with R > 0.95 in this range). The acceptance angles close to 0° correspond to specular reflectance, and the larger angles capture additionally diffuse reflectance.

It can be seen in Fig. 4d that the uncoated NWs have a moderately large specular component, whereas stronger diffuse component is seen from the parylene-C coated NWs. In closer scrutiny, by extrapolation, the specular reflectance is only ≈0.01 with 100 – 200 nm coating, whereas at acceptance angles of 116° - 128° the reflectance is ≈0.1 – 0.15. In other words, with dielectric shells the reflection is >90 % diffuse, whereas without coating the specular component remains significant. This behavior is similar to that observed in the transmittance measurements, and similarly suggests enhanced scattering by the dielectric shells. Previously, low specular reflectance has been reported for dense InP NW arrays [34], while here similar effect is acquired with the parylene-C coating for NWs that initially have moderately high specular reflection component. Finally, it may be observed from Fig. 4d that the increase in observed diffuse reflectance is approximately linear to the increase in the surface area of the corresponding spherical cap and therefore follows Lambertian diffuse reflectance fairly well, as could be expected from randomly-oriented NW forest.

3.4 Photoluminescence

Fig. 5a shows typical photoluminescence (PL) spectra measured from the NWs before and after parylene-C coating (from a spot of approximately 100 µm in diameter). PL emission was observed at ≈860 nm – 925 nm, corresponding to WZ (≈1.42 eV) and ZB (≈1.34 eV) crystal phases [12,35]. The peak position and shape tended more towards 860 nm or 925 nm depending on the measurement area, which indicates variation in crystal structure between different areas on the same sample. This is believed to result from fluctuations in the NW densities, since in denser areas the same precursor flow is divided to a larger amount of Au particles, causing local variations to the growth conditions. The local variations are discussed in more detail in the micro-PL section below.

Fig. 5b shows the relative PL enhancement for each parylene-C shell thickness, i.e., integrated PL intensity from coated NWs divided by uncoated NWs. Overall, the PL intensity follows similar pattern as the absorption in InP (see Fig. 3b) with average enhancement of ≈400 %. In photoluminescence measurements, the excitation light is first absorbed in the NWs, followed by photoluminescence emission. By assuming that absorptivity is equal to emissivity, the total enhancement in PL measurements equals to twice that of absorptance enhancement. The absorption enhancement in InP was ≈200 % (see Fig. 3b) and therefore correlates well with the observed PL enhancement. It should be noted here that the comparably higher enhancements at shell thicknesses of 58 nm and 448 nm were also observed in Fig. 3b, albeit to a smaller degree. It should also be noted that no significant or consistent trend was observed in power-dependent PL measurements with varying shell thickness.

Micro-PL was used to examine the PL properties and shell effects in more detail. Fig. 5c shows microscope images and micro-PL images from NWs with parylene-C shells of 58 nm, 354 nm and 744 nm in thickness. Overall, stronger PL is observed from some NWs than others, pointing towards significant variance in the optical quality even in neighbouring NWs. The thicker shells are clearly visible in microscope

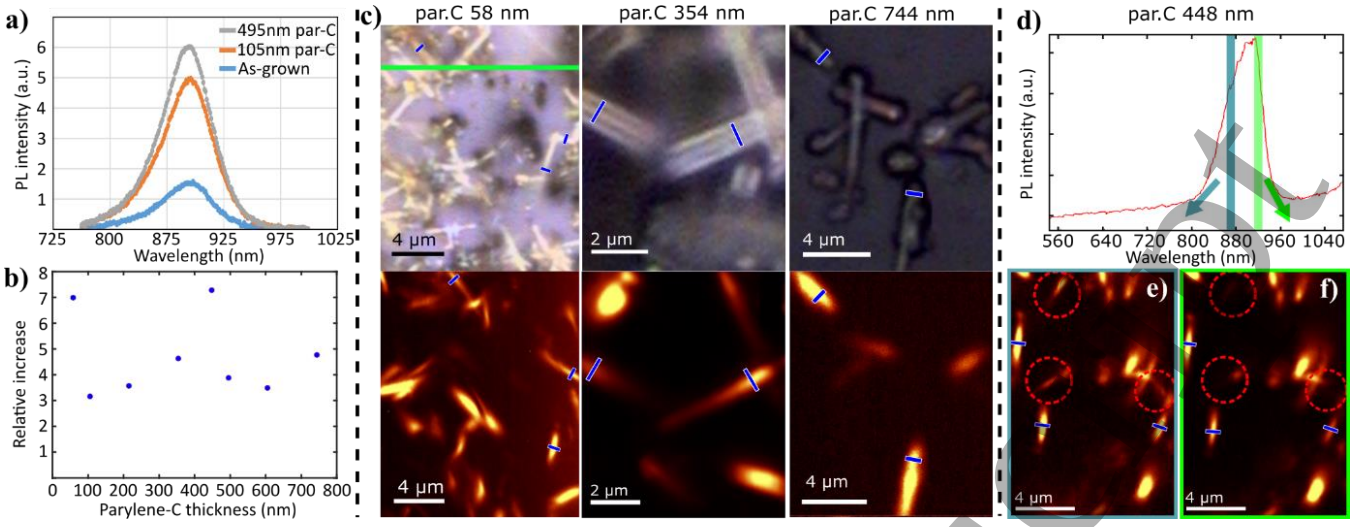

Figure 5: Typical macro-photoluminescence spectra from InP NWs with and without parylene-C shells (a) and relative change in PL intensity at different shell thicknesses (b). Microscope images and corresponding micro-PL photon maps with different shell thicknesses are shown in (c), along with 1µm scale bars (blue) to ease comparison. Typical micro-PL spectrum is shown in (d), collected from areas in (e) and (f), which show photon maps corresponding to ≈870 nm and ≈920 nm wavelength, respectively. The red circles in (e) and (f) highlight NWs that have luminescence at ≈870 nm and not at ≈920 nm.

images and, interestingly, also a larger luminescent area is observed with the thicker shells (see the blue 1 µm-bars in Fig. 5c). This indicates that the dielectric shells induce more diffuse PL emission, similarly to increased diffuse reflectance and diffuse transmittance. For NW device design, the diffuse emission properties may provide a useful tool, or alternatively it may be beneficial to take into account in designs where more directional emission is preferred.

The micro-PL measurements also revealed varying emission characteristics from neighbouring NWs. Fig. 5d shows a micro-PL spectrum measured from the area shown in Fig. 5e-f. The luminescence collected at ≈870 nm (≈1.43 eV, WZ phase) is shown in Fig. 5e and the luminescence collected at ≈920 nm (≈1.35 eV, ZB phase) in Fig. 5f. Majority of the NWs show PL emission at both wavelengths, while a fraction of the NWs (circled in Figs. 5e-f) show luminescence only at ≈870 nm. This suggest that a fraction of the NWs is dominantly WZ, while majority of the NWs are ZB or polytypic (in polytypic NWs the emission is typically below the WZ phase energy [36]). Therefore, the local growth conditions are observed to have significant impact on the NW structure, and variable crystal phase may occur in NWs that are only a few µm apart.

4. Conclusions

In conclusion, thorough optical characterization was carried out on InP NWs grown on glass with and without dielectric parylene-C shells at different thicknesses. The dielectric shells were shown to increase reflectance, decrease transmittance, and increase absorptance. The distribution of light within the structure, *i.e.*, the light that was not reflected or transmitted, was shown to be dominated by InP absorption, while neither Au absorption nor light trapping in the glass growth-substrate were negligible. The dielectric shells were shown to induce stronger diffuse reflectance and transmittance, and to enhance light scattering significantly. Photoluminescence measurements showed that the increased absorption in InP translated to enhanced PL intensity. In micro-PL, the emission was found to be increasingly diffuse with thicker dielectric shells, similarly to as in reflectance and transmittance. Micro-PL also revealed varying crystal structure even in NWs only a few µm apart. Overall, the presented results provide insights on the behaviour and distribution of light in NW arrays on a substrate, as well as effects of dielectric shells. This knowledge delivers a useful tool for light and scattering management in nanoscale engineering, particularly with NWs, using dielectric shells to optimize absorption, emission and scattering.

Supplementary Material

Supplementary material presents: (i) measurement setup schematics, (ii) R,T and 1-R-T data for wavelength range 930 nm – 1600 nm with different parylene-C shell thicknesses, (iii) sample-specific 1-R-T spectra, and (iv) comparison of A (coated NWs) and 1-R-T (as-grown NWs) in long-wavelength range (comparison used to estimate coating effect on Au absorption).

Acknowledgements

The authors acknowledge the Flagship of Photonics Research and Innovation of the Academy of Finland. T.H. acknowledges the financial support by the Finnish Cultural

Foundation and Walter Ahlström Foundation. V.K. acknowledges the support of Aalto University Doctoral School, Walter Ahlström Foundation and Nokia Foundation.

References

[1] Grzela G, Paniagua-Domínguez R, Barten T, Fontana Y, Sánchez-Gil J A and Gómez Rivas J 2012 Nanowire antenna emission *Nano Lett.* **12** 5481–6

[2] Anttu N, Mäntynen H, Sorokina A, Kivisaari P, Sadi T and Lipsanen H 2020 Geometry Tailoring of Emission from Semiconductor Nanowires and Nanocones *Photonics* **7** 23

[3] Wu P M, Anttu N, Xu H Q, Samuelson L and Pistol M-E 2012 Colorful InAs Nanowire Arrays: From Strong to Weak Absorption with Geometrical Tuning *Nano Lett.* **12** 1990–5

[4] Anttu N, Abrand A, Asoli D, Heurlin M, Åberg I, Samuelson L and Borgström M 2014 Absorption of light in InP nanowire arrays *Nano Res.* **7** 816–23

[5] Smyrnakis A, Almpanis E, Constantoudis V, Papanikolaou N and Gogolides E 2015 Optical properties of high aspect ratio plasma etched silicon nanowires: Fabrication-induced variability dramatically reduces reflectance *Nanotechnology* **26** 085301

[6] Tsakalakos L, Balch J, Fronheiser J, Korevaar B A, Sulima O and Rand J 2007 Silicon nanowire solar cells *Appl. Phys. Lett.* **91** 233117

[7] Raj V, Vora K, Fu L, Tan H H and Jagadish C 2019 High-Efficiency Solar Cells from Extremely Low Minority Carrier Lifetime Substrates Using Radial Junction Nanowire Architecture *ACS Nano* **13** 12015–23

[8] Aberg I, Vescovi G, Asoli D, Naseem U, Gilboy J P, Sundvall C, Dahlgren A, Svensson K E, Anttu N, Bjork M T and Samuelson L 2016 A GaAs Nanowire Array Solar Cell With 15.3% Efficiency at 1 Sun *IEEE J. Photovoltaics* **6** 185–90

[9] Wallentin J, Anttu N, Asoli D, Huffman M, Aberg I, Magnusson M H, Siefer G, Fuss-Kailuweit P, Dimroth F, Witzigmann B, Xu H Q, Samuelson L, Deppert K and Borgström M T 2013 InP nanowire array solar cells achieving 13.8% efficiency by exceeding the ray optics limit. *Science* **339** 1057–60

[10] Dhaka V, Pale V, Khayrudinov V, Kakko J P, Haggren T, Jiang H, Kauppinen E and Lipsanen H 2016 Synthesis and properties of ultra-long InP nanowires on glass *Nanotechnology* **27** 505606

[11] Blumberg C, Liborius L, Ackermann J, Tegude F J, Poloczek A, Prost W and Weimann N 2020 Spatially controlled VLS epitaxy of gallium arsenide nanowires on gallium nitride layers *CrystEngComm* **22** 1239–50

[12] Kauppinen C, Haggren T, Lipsanen H and Sopanen M 2020 Metalorganic vapor phase epitaxy of wurtzite InP nanowires on GaN *Appl. Phys. Lett.* **116** 093101

[13] Haggren T, Perros A, Dhaka V, Huhtio T, Jussila H, Jiang H, Ruoho M, Kakko J-P J P, Kauppinen E and Lipsanen H 2013 GaAs nanowires grown on Al-doped ZnO buffer layer *J. Appl. Phys.* **114** 084309

[14] Wu D, Tang X H, Olivier A and Li X Q 2015 Free-standing GaAs nanowires growth on ITO glass by MOCVD *Mater. Res. Express* **2** 045002

[15] Anttu N, Dagytė V, Zeng X, Otnes G and Borgström M 2017 Absorption and transmission of light in III–V nanowire arrays for tandem solar cell applications *Nanotechnology* **28** 205203

[16] Muskens O L, Diedenhofen S L, Kaas B C, Algra R E, Bakkers E P A M, Gómez Rivas J and Lagendijk A 2009 Large Photonic Strength of Highly Tunable Resonant Nanowire Materials *Nano Lett.* **9** 930–4

[17] Anttu N, Namazi K L, Wu P M, Yang P, Xu H, Xu H Q and Håkanson U 2012 Drastically increased absorption in vertical semiconductor nanowire arrays: A non-absorbing dielectric shell makes the difference *Nano Res.* **5** 863–74

[18] Winnerl J, Kraut M, Hudeczek R and Stutzmann M 2019 GaN nanowire arrays for photocatalytic applications II: influence of a dielectric shell and liquid environments *Appl. Phys. B Lasers Opt.* **125** 77

[19] Zhong Z, Li Z, Gao Q, Li Z, Peng K, Li L, Mokkapati S, Vora K, Wu J, Zhang G, Wang Z, Fu L, Tan H H and Jagadish C 2016 Efficiency enhancement of axial junction InP single nanowire solar cells by dielectric coating *Nano Energy* **28** 106–14

[20] Leiterer C, Brönstrup G, Jahr N, Talkenberg F, Radnóczi G Z, Pécz B, Christiansen S and Sivakov V 2016 Index matching at the nanoscale: Light scattering by core-shell Si/SiO x nanowires *Nanotechnology* **27** 435202

[21] Li X, Shi T, Liu G, Wen L, Zhou B and Wang Y 2015 Absorption enhancement of GaInP nanowires by tailoring transparent shell thicknesses and its application in III-V nanowire/Si film two-junction solar cells *Opt. Express* **23** 25316

[22] Haggren T, Shah A, Autere A, Kakko J-P J-P, Dhaka V, Kim M, Huhtio T, Sun Z and Lipsanen H 2017 Nanowire encapsulation with polymer for electrical isolation and enhanced optical properties *Nano Res.* **10** 2657–66

[23] Ahn Y, Lee D, Jeong Y, Lee H and Lee Y 2017 Flexible metal nanowire-parylene C transparent electrodes for next generation optoelectronic devices *J. Mater. Chem. C* **5** 2425–31

[24] Wu W, Wen X and Wang Z L 2013 Taxel-addressable matrix of vertical-nanowire piezotronic transistors for active and adaptive tactile imaging *Science (80-.).* **340** 952–7

[25] Chen C L, Lopez E, Makaram P, Selvarasah S, Busnaina A, Jung Y J, Müftü S and Dokmeci M R 2007 Fabrication and evaluation of Carbon Nanotube-Parylene functional composite-films *TRANSDUCERS and EUROSENSORS '07 - 4th International Conference on Solid-State Sensors, Actuators and Microsystems* pp 1019–22

[26] Aji A S, Solís-Fernández P, Ji H G, Fukuda K and Ago H 2017 High Mobility WS_2 Transistors Realized by Multilayer Graphene Electrodes and Application to High Responsivity Flexible Photodetectors *Adv. Funct. Mater.* **27** 1703448

[27] Fukuda K, Takeda Y, Yoshimura Y, Shiwaku R, Tran L T, Sekine T, Mizukami M, Kumaki D and Tokito S 2014 Fully-printed high-performance organic thin-film transistors and circuitry on one-micron-thick polymer films *Nat. Commun.* **5** 1–8

[28] Wiersma D S 2008 The physics and applications of random lasers *Nat. Phys.* **4** 359–67

[29] Lerosey G, De Rosny J, Tourin A and Fink M 2007 Focusing beyond the diffraction limit with far-field time reversal *Science (80-.).* **315** 1120–2

[30] Jeong Y ., Ratier B, Moliton A and Guyard L 2002 UV–visible and infrared characterization of poly(p-xylylene) films for waveguide applications and OLED encapsulation *Synth. Met.* **127** 189–93

[31] Gaynor J F and Desu S B 2011 Optical properties of polymeric thin films grown by chemical vapor deposition *J. Mater. Res.* **11** 236–42

[32] Lee J H, Kim U J, Han C H, Rha S K, Lee W J and Park C O 2004 Investigation of silicon oxide thin films prepared by atomic layer deposition using SiH2Cl2 and O3 as the precursors *Japanese J. Appl. Physics, Part 2 Lett.* **43** L328

[33] Wang Z Y, Zhang R J, Lu H L, Chen X, Sun Y, Zhang Y, Wei Y F, Xu J P, Wang S Y, Zheng Y X and Chen L Y 2015 The impact of thickness and thermal annealing on refractive index for aluminum oxide thin films deposited by atomic layer deposition *Nanoscale Res. Lett.* **10** 1–6

[34] Muskens O L, Rivas J G, Algra R E, Bakkers E P A M and Lagendijk A 2008 Design of Light Scattering in Nanowire Materials for Photovoltaic Applications *Nano Lett.* **8** 2638–42

[35] Mattila M, Hakkarainen T, Mulot M and Lipsanen H 2006 Crystal-structure-dependent photoluminescence from InP nanowires *Nanotechnology* **17** 1580–3

[36] Ikejiri K, Kitauchi Y, Tomioka K, Motohisa J and Fukui T 2011 Zinc blende and wurtzite crystal phase mixing and transition in indium phosphide nanowires *Nano Lett.* **11** 4314–8